

Direct nanofabrication and transmission electron microscopy on a suite of easy-to-prepare ultrathin film substrates

Daniel B. Allred^a, Melvin T. Zin^b, Hong Ma^b, Mehmet Sarikaya^b, François Baneyx^a, Alex K.-Y. Jen^b, Daniel T. Schwartz^{a,*}

^a Department of Chemical Engineering, University of Washington, Box 351750, Seattle, WA, 98195, USA

^b Department of Materials Science and Engineering, University of Washington, Box 352120 Seattle, WA, 98195, USA

Received 14 July 2006; received in revised form 5 December 2006; accepted 11 January 2007

Available online 23 January 2007

Abstract

A high-yield, easy to master method for preparing electron transparent metal, oxide, and carbon ultrathin film substrates suitable for direct nano/micro-fabrication and transmission electron microscopy (TEM) is presented. To demonstrate the versatility of these substrates for fabrication processes, we use e-beam lithography, self-assembled colloidal and protein templates, and microcontact printing to create patterned masks for subsequent electrodeposition of two dimensional and three dimensional structures. The electrodeposited structures range in scale from a few nanometers to a few micrometers in characteristic dimensions. Because fabrication occurs directly on ultrathin films, TEM analysis of the resulting materials and buried interfaces is straightforward without any destructive sample preparation. We show that all the normal TEM analytical methods (imaging, diffraction, electron and X-ray spectroscopies) are compatible with the fabricated structures and the thin film substrates. These electron transparent substrates have largely rendered the need for TEM sample preparation on fabricated structures obsolete in our lab. © 2007 Elsevier B.V. All rights reserved.

Keywords: Electrodeposition; Template; Metal films; Electron transparent; Lithography; Protein; Transmission electron microscopy (TEM)

1. Introduction

Fabrication of thin film structures and devices with lateral dimensions well below 100 nm is routine [1], though nondestructive characterization of the buried materials and interfaces in these structures often is not. Transmission electron microscopy (TEM), in theory, is the ideal tool for analyzing the composition and structure of many fabricated nanostructures. In practice, however, most thin film devices are fabricated on electron opaque substrates, forcing the use of destructive sample cross-sectioning or milling methods to analyze interesting buried materials and interfaces. Cross-sectioning for TEM is generally tedious and it also can introduce artifacts [2–4].

The availability of a low cost suite of ultrathin film substrates suitable for nano/microfabrication and TEM would represent the ideal link between the outstanding traits of TEM and the unfortunate practicalities of sample preparation. Currently, one can purchase TEM grids with electron-transparent ultrathin film carbon, silicon dioxide, and silicon nitride films. In our group, we are especially interested in studying electrochemical micro and nanofabrication using electrodeposition combined with self-assembled or lithographically-defined masks. Carbon substrates (because they are conductive) are often used to study electrochemical growth processes [5–8]. However, carbon surfaces are not generally used in fabrication processes because their low surface energies lead to poor nucleation densities and low-quality filling of space in masks. Current methods for making and using high surface energy ultrathin films (e.g., from noble metals) are impractical as an electron-transparent substrate for routine fabrication; typically the films, themselves, are the subject of study [9]. Recently, a new microdevice for *in situ* TEM imaging of electrochemical

* Corresponding author. Tel.: +1 206 685 4815; fax: +1 206 543 3778.

E-mail address: dts@u.washington.edu (D.T. Schwartz).

nucleation on gold-coated silicon nitride was described [10]. The device architecture was fairly complex, in order to perform *in situ* studies, impairing image resolution. Nonetheless, it demonstrated the high level of insights possible when plan view TEM is combined with electrodeposition. Creating easy-to-use methods that allow complex nanofabrication and sample-preparation-free TEM characterization of the resulting buried materials and interfaces is a key step in the advancement of nanodevice science and technology.

Here, we describe a simple and robust way to create freestanding electron transparent substrates that are suitable for nanoscale fabrication. We first used these films with protein-templated electrodeposition [11], but here we extend their generality by making freestanding metal, metal oxide, and nonmetal film substrates, and then use e-beam lithography, soft lithography, as well as colloidal crystal templates to pattern materials grown by electrodeposition. The preparation of these ultrathin films is sufficiently fast and easy that it can be mastered quickly. With these electron transparent substrates, fabrication at the nanoscale is routine and so is nondestructive plan-view TEM analysis of the materials and structures that are built on them.

2. Methods and materials

2.1. Preparation of electron-transparent metal films

A modification of the soap on glass slide technique used by Carpenter and Curcio [12] was used. Briefly, a permanent marker or a sugar–aerosol solution (48 g sucrose added per L of 2% aqueous sodium dioctyl sulfosuccinate) was used to define regions on glass slides which were then sputter-coated with the desired metal by argon-ion sputtering according to the manufacturer's instructions (SPI Sputter-Coater or Gatan Model 682 Precision Etching Coating System). Metal films were then freed in methanol and picked up onto gold TEM grids (200, 300, or 400 square or hexagonal mesh, SPI Supplies). Batches of five to twelve were made at a time. Film thicknesses are estimated to be 1–3 nm based on quartz crystal microbalance monitoring and optical density comparisons. A significantly higher throughput technique with better product uniformity and reproducibility is the subject of a patent filed with the U.S. Patent Office [13].

2.2. Assembly of latex spheres

Monodisperse (1–2% standard deviation) polystyrene latex spheres from Duke Scientific corporation (Nanosphere size standard, sizes as reported) were used for preparing templates. They were assembled by mixing 1–2 μL of stock suspension with 5 μL of water and applying onto metal-coated TEM grids then allowed to air dry.

2.3. Preparation of protein templates

Protein templates were prepared by applying 1–2 μL of a 1 mg/mL in 5% sodium dodecyl sulfate stock solution of

purified S-layer proteins from *Deinococcus radiodurans* as previously reported [11] onto metal coated TEM grids.

2.4. Microcontact printing

Micropatterned photoresist film, fabricated by photolithography, was used as a master to replicate stamps for microcontact printing (μCP). Masters were coated with (1, 1, 2, 2-tetrahydroperfluorodecyl)trichlorosilane (Sigma–Aldrich) to ensure a clean release of the cured stamp. A typical stamp was made by casting a 10:1 (v/v) mixture of polydimethyl siloxane and curing agent (Sylgard 184, Dow Corning, Midland, MI) against a silanized master for 2 days at room temperature in ambient conditions. Stamps were used as the cast and the surface chemistry of the stamp was not modified. Inking was done by covering the patterned side of the stamp with an ethanolic solution (200 proof, Aaper Alcohol and Chemical Company) of octadecanethiol (Sigma–Aldrich) for 1 min. The inked stamp was dried in nitrogen and brought into a conformal contact with the surface by hand for ~ 20 s. μCP was performed on films before floating off onto TEM grids. Alternatively, μCP can also be performed on grids immobilized on solidified sugar–aerosol solution (as described in Preparation of electron-transparent metal films above).

2.5. Electron-beam lithography

Electron-beam lithography was performed by spin-coating a 3% solution of 950K polymethylmethacrylate (PMMA) in anisole on grids immobilized on solidified sugar–aerosol solution (as described in Preparation of electron-transparent metal films above) at 2000 rpm for 45 s. Grids were subsequently freed by cutting around the edge with a razor blade and allowing the surfactant to be dissolved away with water. Pattern generation was performed on a JEOL 7000 SEM at 30 kV using the Nanometer Pattern Generation System (NPGS) from JC Nability Lithography Systems using a 35 pA beam current at 7 mm working distance. Development was performed in 3:1 isopropanol:methyl isobutyl ketone and rinsed in isopropanol and the resist was removed in acetone after electrodeposition.

2.6. Electrodeposition

Electrodeposition was performed potentiostatically using a PAR 273A Potentiostat in a small glass beaker of the desired electrolyte with a platinum counter electrode and a saturated calomel electrode (SCE) or saturated sodium calomel electrode (SSCE). All potentials are reported versus the SCE and all experiments were performed at room temperature in ambient air. The metal-coated TEM grid was the working electrode; electrical contact was made by self-closing anti-capillary tweezers at an acute angle to the electrolyte surface so that the meniscus contacted the mask-covered sized of the surface only. The approach to the electrolyte surface was performed carefully using a *z*-axis

stage to prevent accidental electrolyte contact with the tweezers. Cuprous oxide was electrodeposited for 10–15 min at -450 mV vs. SCE in a Stareck [14] electrolyte of 0.4 M cupric sulfate, 3.0 M lactic acid, made to pH 9 with sodium hydroxide following the work of Zhou and Switzer [15]. Copper was electrodeposited for 3 s at -300 mV vs. SCE in 0.5 M cupric sulfate, 0.5 M sulfuric acid. Cobalt was electrodeposited for 2 s at -1.1 V vs. SCE in 1.5 M cobalt sulfate, 0.6 M boric acid. For pulse-plating through e-beam lithography masks an on–off cycle was performed with 1-sec on and 3-sec off for 4 cycles.

2.7. Electron microscopy

A JEOL 7000 SEM at 30 kV was used for scanning electron microscopy. A Phillips 420 TEM, $C_s \sim 1.3$ mm, 120 kV was used for transmission electron microscopy. Electron diffraction was calibrated with an aluminum foil standard. Negatives were scanned with an EPSON backlit scanner and inverted digitally. Electron spectroscopy work was performed on a JEOL 2010, $C_s \sim 0.5$ mm, at 200 kV in the Environmental Molecular Sciences Laboratory at Pacific Northwest National Laboratory.

3. Results and discussion

We report on the preparation of freestanding electron transparent films for 11 different materials. The films are typically between 2 and 3 nm thick and are supported by an underlying grid with 40- μ m square windows. We have found that thinner films often do not have good material properties and thicker films become too coarse-grained for high magnification imaging. Fig. 1A shows a scanning electron microscopy (SEM) image of the grid support structure with a platinum film covering the grid. The supporting grid is being imaged through the film, indicating its transparency at the modest 25 keV accelerating voltage of the SEM used. The film is more transparent at the higher accelerating voltages typical in TEM. The black arrow in Fig. 1A points to a small cluster of 1.6 μ m silica beads that have been placed on the film to highlight it, and the white arrow points to a defect in the freestanding Pt film. Approximately 3% of the usable area in these freestanding films are damaged.

Fig. 1B compares the bright field/dark field TEM images for AuPd alloy (60–40) and Pt films at high magnification. The AuPd and Pt films are nanocrystalline, with characteristic crystallite sizes of 2–5 nm. Electron diffraction of the structures we fabricate on these substrates display a weak, broad background diffraction from the nanocrystalline nature of the film (as discussed below). The absolute transparency of each film can be evaluated by comparing the transmitted electron intensity in damaged areas (without film) to areas that are film covered. We find that the AuPd and Pt films shown in Fig. 1A and B are among the least transparent we make, though their surface properties are necessary for the application intended in this specific demonstration.

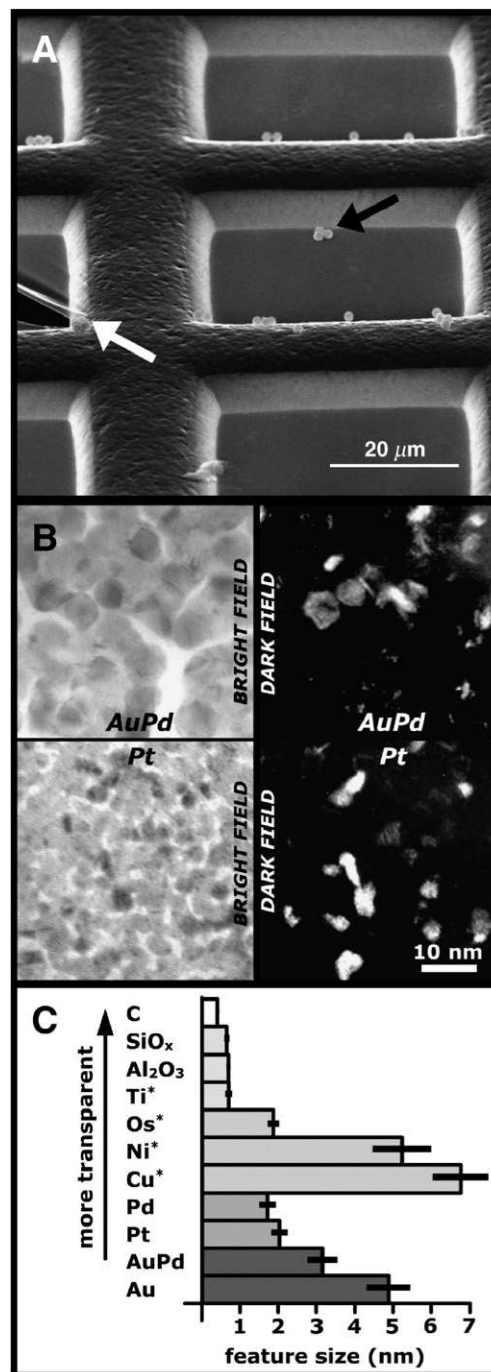


Fig. 1. A) SEM image of a platinum-coated TEM grid supporting 1.6 μ m silica particles. (black arrow) The tear in the film (white arrow) reveals the electron transparency at 30 kV. B) TEM images of AuPd and Pt films in bright field (left) and dark field (right). C) Comparison of film structure and relative transparency for a suite of materials prepared the method described here. Feature sizes (not crystallite sizes) are measured using image analysis software ImageJ (National Institute of Health, United States), whereas the relative electron transparency is qualitatively ordered. Films are all about 2 nm thick except carbon, which is about 10 nm thick, and silica and alumina, each about 30 nm thick. Asterisks denote films which were prepared as metals but oxidize upon exposure to air; the surface state of carbon films was not evaluated.

As noted in the Methods and materials section, all the films were formed by sputtering on sacrificial sugar–aerosol or permanent marker coated surfaces, and then

freed in methanol to be picked up onto the 3 mm diameter grids. Fig. 1C summarizes results for the characteristic feature size and electron transparency of the eleven different electron transparent substrates we have made using these methods.

Material growth by electrodeposition is a challenging test for the mechanical robustness of these films, as capillary

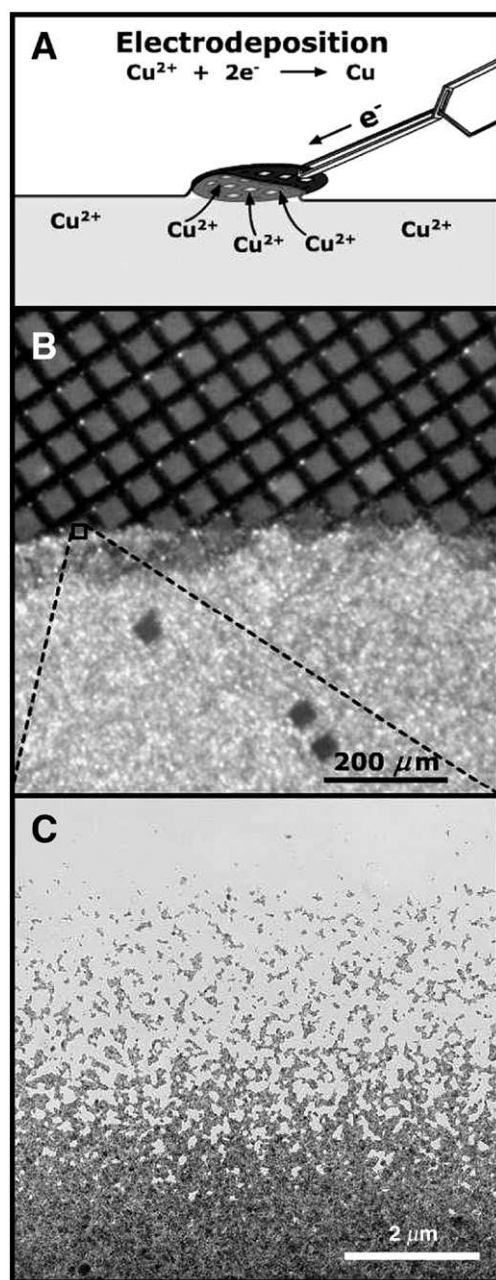


Fig. 2. A) Schematic of the typical method for handling ultrathin metal films for electrochemical fabrication processes. Electrical contact is made by self-closing anti-capillary tweezers. A counter electrode (not shown) is typically oriented parallel to the grid to maintain perpendicular electrical field lines to the surface. B) Optical image of copper electrodeposited onto half of a platinum coated TEM grid using method shown in (A). C) TEM image of the copper deposit formed at the air–water interface as illustrated in the boxed area in (B).

forces tend to destroy fragile structures at these length scales. The basic protocol that we have adopted is to make electrical contact to the thin metal film by gripping the grid with self-closing tweezers and lowering the grid to the electrolyte surface at an acute angle such that the meniscus only contacts the desired side of the grid, as illustrated in Fig. 2A. This arrangement ensures deposition on only one side of the grid, which is important when depositing material through masks made by lithography or self-assembly techniques. The counter electrode can be positioned for optimal electric field uniformity [16]. This arrangement is easily customized for three-electrode cells with a reference electrode, as well as use of a controlled environment cell. Fig. 2B shows an optical micrograph of copper electrodeposited onto part of a freestanding platinum-film substrate. Within the view of Fig. 2B, we can see a total of five $40 \times 40 \mu\text{m}$ grid windows that are damaged (out of roughly 230 that are visible). This is approximately the number of damaged windows we see before electrochemical processing (about 3%), showing that the film withstood capillary forces upon immersion into and emersion from the electrolyte. The TEM image of Fig. 2C is taken near the meniscus where the deposit interface is diffuse. No sample preparation was needed to examine this deposit.

In the process of through-mask electrodeposition, the mask must provide an insulating barrier against nucleation and growth of material, resulting in localized growth in the unmasked regions [17]. Fig. 3A and B demonstrate mask fabrication using soft lithography and electron-beam lithography on ultrathin noble metal substrates, followed by electrodeposition of copper and cobalt, respectively. No subsequent sample preparation was needed to directly image the patterned deposits in the TEM. In order to adapt these well-established patterning technologies to the highly-flexible and fragile ultrathin substrates, we have found it necessary to first immobilize the films using a sugar–aerosol solution as an adhesive (see Methods and materials). Microcontact printing of patterned alkanethiols can be performed on the immobilized grid, followed by release of the self assembled monolayer patterned grid. Subsequent electrodeposition results in a patterned deposit (Fig. 3A) similar to that obtained using soft lithography on conventional substrates [18]. Electron-beam lithography is a serial pattern generation process often used in the construction of photomasks for deep UV lithography or, in rare cases, for direct fabrication. Here, adhesive immobilization with solidified sugar–aerosol is used to attach the film-coated grid to a larger substrate that is more suited to spin-coating the polymethylmethacrylate (PMMA) electron-beam resist. After spin coating, the grid is recovered and subsequent steps (writing, developing, pulse-plating, mask dissolution) are performed in the usual manner, resulting in the patterned cobalt seen in Fig. 3B.

Self-assembling templates such as colloidal latex spheres also can be readily cast onto these ultrathin films where they spontaneously order owing to capillary interactions during drying. Electrodeposition fills space around the crystalline colloidal template, generating a three-dimensional inverse opal

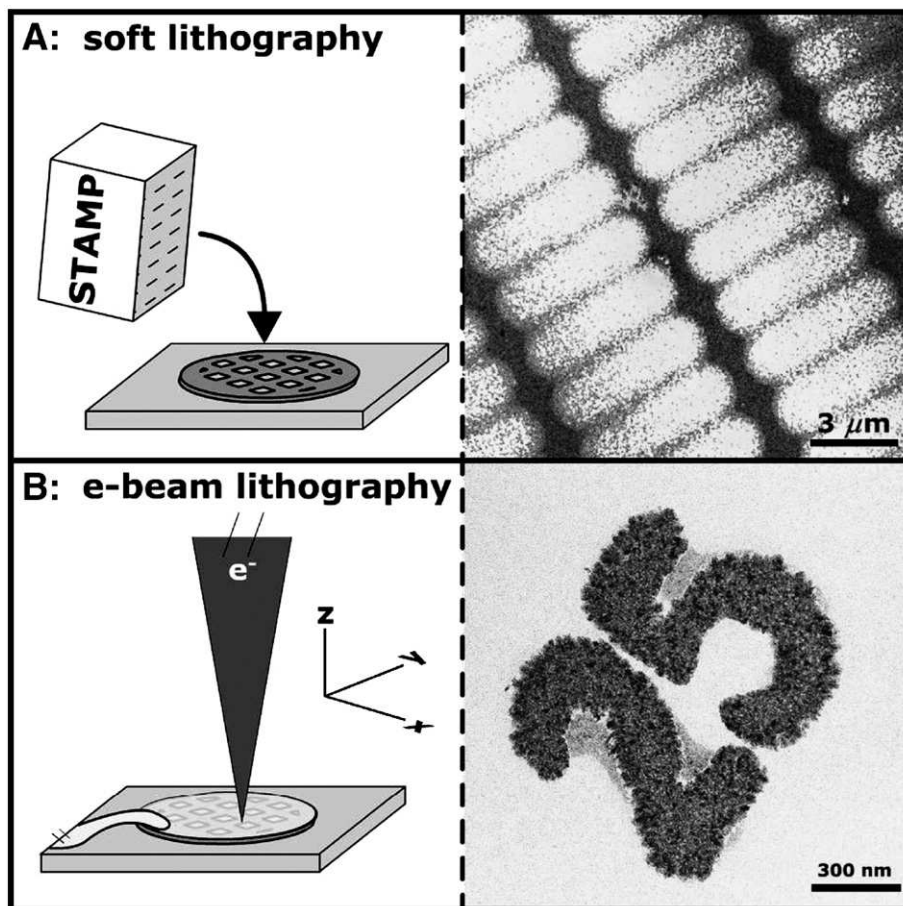


Fig. 3. A) Microcontact printing, a soft-lithography technique, is used to create a patterned alkanethiol mask (light regions) on the AuPd ultrathin film where copper (dark regions) does not grow. B) Electron-beam lithography is used to write an opening in PMMA, allowing subsequent electrodeposition of cobalt on the Pt ultrathin film. The plan-view TEM images on the right were both acquired immediately after the fabrication process, with no sample preparation needed.

structure [19,20]. Fig. 4 shows TEM images obtained from partially-ordered latex spheres cast on an ultrathin AuPd film before and after electrodeposition of ~ 50 nm of cuprous oxide (Cu_2O). Note that in the “after” image, electron dense Cu_2O is seen filling in voids where the 240 nm spheres are close-packed, as well as the open “defect” regions where there are no latex spheres. The spheres have not been removed in the “after” image. Because the latex spheres have rather low electron density, we are able to use transmission-based imaging to see exactly where the cuprous oxide is filling space, even though much of the material growth occurs beneath the latex sphere layer. To the best of our knowledge, this is the first direct, non-destructive, imaging of initial film growth through a colloidal crystal template (normally, one dissolves the latex template to see the patterned deposit). Because we do not need to remove the template (or other organic masks as in Fig. 3), it is possible to evaluate a sample and then reinsert it into the fabrication process.

The results in Figs. 3 and 4 suggest that entire devices can be built and evaluated nondestructively, as long as they fit in the microscope and remain sufficiently electron transparent to see the buried materials and interfaces (perhaps a total device thickness around ~ 100 nm for many of the inorganic

materials used in semiconductor devices, depending on specifics of the materials and the accelerating voltages). Moreover, with high-tilt stages and modern tomography software, cross-sections are no longer needed because one can digitally “slice” through any desired region of a three-dimensionally reconstructed image to look for inclusions, voids, pits, etc.

The prior figures have emphasized the compatibility of our ultrathin film substrates with various fabrication methods, using TEM imaging to characterize the structures. However, TEM can be used for more sophisticated diagnostics than pure imaging. Fig. 5A shows the use of a crystalline bacterial cell surface protein mask to pattern on ultrathin AuPd substrates with a hexagonal Cu_2O nanostructure (18 nm periodicity and nanometer-scale feature sizes). The top left region, labeled (i) has crystalline protein present, resulting in an ordered hexagonal domain of Cu_2O . The top right region contains none of the protein, resulting in a uniform thin film of Cu_2O with no hexagonal superstructure. The lower portion of the image, labeled (ii), is the bare AuPd ultrathin film substrate. Fig. 5B shows the use of electron energy loss spectroscopy (EELS) for characterizing the elemental composition of regions (i) and (ii). Clearly, the spectra in Fig. 5B

show that region (i), the nanostructured region, is rich in copper compared to region (ii), a result also confirmed by energy dispersive X-ray spectroscopy (another TEM diagnostic, not shown). However, the presence of copper signal in region (i) does not, on its own, confirm that the nanostructured deposit is Cu_2O , as presumed. To further analyze the deposit, electron diffraction was also performed in the two regions, as shown in Fig. 5C. Region (i) revealed an assortment of individual crystals (one of which was recognized as Cu_2O in the [211] orientation, indicated by dashed lines) whereas region (ii) contained very few crystals of any significant size (this was typical for as-produced AuPd films). Diffraction over larger areas (not shown) as well as dark-field imaging revealed that cuprous oxide particles were not confined merely to the selected regions, but were instead evenly distributed throughout all electron dense regions with randomly oriented grains. In summary, the combined capabilities of imaging, diffraction, and spectroscopy make plan-view TEM a complete and straightforward tool for the

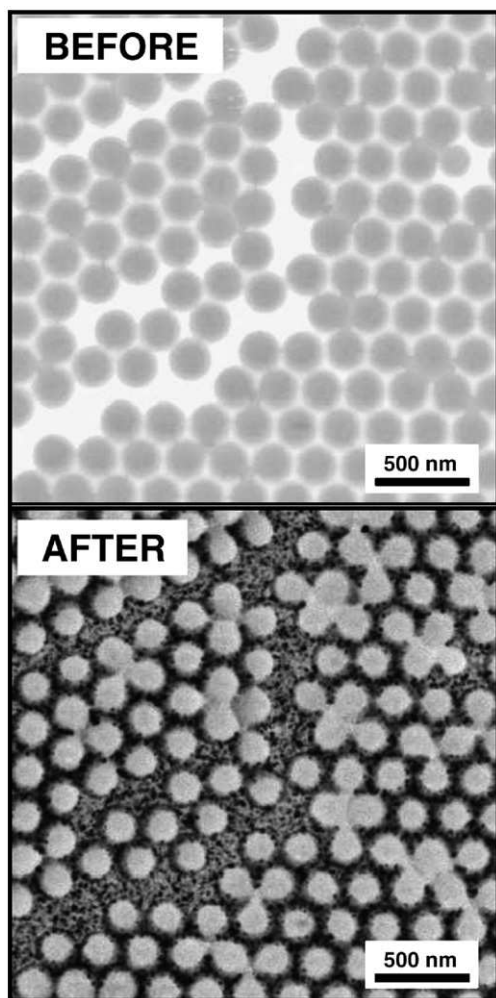


Fig. 4. The BEFORE image is a TEM micrograph showing 240 nm latex spheres (light gray) that have been cast on a AuPd film. The AFTER image shows the same region following electrodeposition of ~ 50 nm of Cu_2O ; the latex spheres remain on the surface.

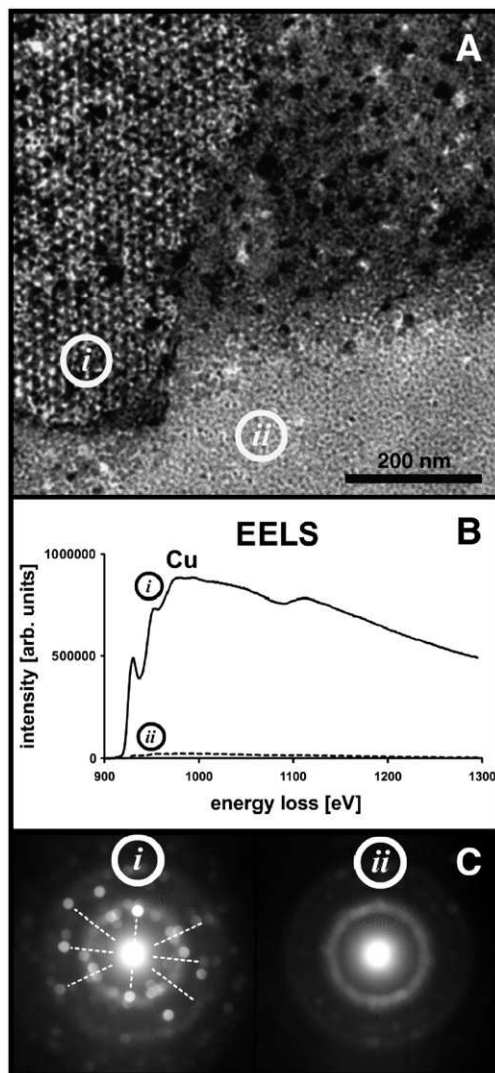


Fig. 5. A) TEM image of cuprous oxide electrodeposited on AuPd through crystalline hexagonally-packed intermediate layer proteins from *Deinococcus radiodurans*. Electron spectra and diffraction were acquired in protein nanostructured region labelled (i) and the bare AuPd substrate region labelled (ii). B) EELS spectra from regions (i) and (ii) after background subtraction. C) Converging beam electron diffraction patterns. Region (i) contains an assortment of many small crystals, at least one of which can be recognized as a single crystal and indexed to match cuprous oxide along the (211) zone axis. Region (ii) contains mostly diffraction rings with too few diffractions spots to be indexed to an individual crystal; this is typical for bare the as-prepared AuPd ultrathin film substrates. The AuPd substrate signal is also superimposed in region (i), as expected in transmission.

analysis of micro and nanofabricated structures on these ultrathin film substrates.

4. Conclusions

We have presented a method for preparing a suite of electron transparent ultrathin films substrates from a wide variety of materials. It is shown that the ultrathin film substrates are compatible with electrochemical nano and microfabrication using soft lithography, e-beam lithography, and self assembling colloidal and protein templates. Because the substrates are

already electron transparent and made of technologically useful materials, they marry the best traits of transmission electron imaging, diffraction, and spectroscopy with fabrication processes. As a result of these robust ultrathin film substrates, transmission electron microscopy has now become our most productive method for exploring nanofabricated structures in two and three dimensions.

Acknowledgments

DA is grateful to Phil Bartlett and Mamdouh Abdelsalem at the University of Southampton for experience in templated electrodeposition funded by a Worldwide Universities Network Global Exchange Fellowship. DA also personally acknowledges Haixia Dai and Hanson Fong for general helpful discussions. This work was partially supported by the U.S. Army Research Office—Defense University Research Initiative in NanoTechnology (DAAD19-01-1-04999), the National Science Foundation (DGE-9987620, DMR-0520567), and the Boeing–Sutter Endowment. Electron spectroscopy work was performed in the Environmental Molecular Sciences Laboratory, a national scientific user facility sponsored by the Department of Energy's Office of Biological and Environmental Research and located at Pacific Northwest National Laboratory.

References

- [1] J. Sone, J. Fujita, Y. Ochiai, S. Manako, S. Matsui, E. Nomura, T. Baba, H. Kawaura, T. Sakamoto, C.D. Chen, Y. Nakamura, J.S. Tsai, *Nanotechnology* 10 (1999) 135.
- [2] L.D. Madsen, L. Weaver, S.N. Jacobsen, *Microsc. Res. Tech.* 36 (1997) 354.
- [3] J.C.H. Spence, *Mater. Sci. Eng. R* 26 (1999) 1.
- [4] A.C. Wright, *Ultramicroscopy* 83 (2000) 1.
- [5] F. Favier, E.C. Walter, M.P. Zach, T. Benter, R.M. Penner, *Science* 293 (2001) 2227.
- [6] D.-L. Lu, K. Tanaka, *J. Electrochem. Soc.* 143 (1996) 2105.
- [7] M.P. Zach, K. Inazu, K.H. Ng, J.C. Hemminger, R.M. Penner, *Chem. Mater.* 14 (2002) 3206.
- [8] J.V. Zoval, J. Lee, S. Gorer, R.M. Penner, *J. Phys. Chem. B* 102 (1998) 1166.
- [9] C.A.P. Leite, F. Galebeck, *J. Colloid Interf. Sci.* 235 (2001) 4.
- [10] M.J. Williamson, R.M. Tromp, P.M. Vereecken, R. Hull, F.M. Ross, *Nat. Mater.* 2 (2003) 532.
- [11] D.B. Allred, M. Sarikaya, F. Baneyx, D.T. Schwartz, *Nano Lett.* 5 (2005) 609.
- [12] F.E. Carpenter, J.A. Curcio, *Rev. Sci. Instrum.* 21 (1950) 675.
- [13] D.B. Allred, D.T. Schwartz, US Patent (filed Dec. 14, 2005).
- [14] J.E. Stareck, US Patent #2,081,121, (1937).
- [15] Y.C. Zhou, J.A. Switzer, *Script. Mater.* 38 (1998) 1731.
- [16] M. Datta, D. Landolt, *Electrochim. Acta* 45 (2000) 2535.
- [17] L.T. Romankiw, *Electrochim. Acta* 42 (1997) 2985.
- [18] C.B. Gorman, H.A. Biebuyck, G.M. Whitesides, *Chem. Mater.* 7 (1995) 526.
- [19] P.N. Bartlett, P.R. Birkin, M.A. Ghanem, *Chem. Commun.* 1 (2000) 1671.
- [20] P.V. Braun, P. Wiltzius, *Nature* 402 (1999) 603.